Powder Technology 286 (2015) 828–837

Contents lists available at ScienceDirect

Powder Technology

journal homepage: www.elsevier.com/locate/powtec

Decrease in mutual interference among particles with increasing cluster void ratio

Kenji Nakashima [a,*], Yuuki Johno [b], Fuminori Matsuyama [c], Toshinobu Shigematsu [d]

[a] Department of Mechanical Engineering, Toyohashi University of Technology, 1-1 Hibarigaoka, Tempaku, Toyohashi, Aichi 441-8580, Japan
[b] Department of Chemical and Biological Engineering, National Institute of Technology, Sasebo College, 1-1 Okishin, Sasebo, Nagasaki 857-1193, Japan
[c] Department of Mechanical Engineering, National Institute of Technology, Sasebo College, 1-1 Okishin, Sasebo, Nagasaki 857-1193, Japan
[d] Department of Control Engineering, National Institute of Technology, Sasebo College, 1-1 Okishin, Sasebo, Nagasaki 857-1193, Japan

ARTICLE INFO

Article history:
Received 16 June 2015
Received in revised form 11 September 2015
Accepted 18 September 2015
Available online 21 September 2015

Keywords:
Gas–particle two-phase flow
Direct numerical simulation
Particle cluster
Powder scattering
Void ratio

ABSTRACT

Objective: When a powder suspension in a flow inhomogeneously disperses, the particles form a cluster. Cluster is defined as the state where the fluid and particles move together through mutual fluid–dynamic interference. This represents a middle state between the lean scatter state, which is considered to be similar to single-particle sedimentation, and the agglomerate state. This study investigates the critical void ratio of the change from the cluster state to a lean scatter state.
Design: Direct numerical simulations of a spherical particle cluster subjected to a uniform flow are performed, and the influence of the flow on the cluster under various void ratios is analyzed based on the calculation results.
Methods: The relationship between the cluster void ratio (or particle volume fraction) and relative velocity between the flow and cluster, flow structure observed in visualization maps, velocity distribution of air flow passing through a cluster, and the fluid–dynamic energy budget were analyzed.
Results: (i) When the void ratio of a particle cluster ε shifts from 0.96 to a higher value of 0.98, the mutual interference effect is lost and the powder suddenly shifts to a lean scatter state. (ii) The kinetic energy of the cluster and particle volume fraction $\phi(=1-\varepsilon)$ are inversely proportional. (iii) With regard to the fluid–dynamic energy budget around the cluster immediately after being subjected to air flow, a very strong mutual interference is confirmed (i.e., the cluster is similar to a rigid body) when $\varepsilon = 0.850$. At $\varepsilon = 0.998$ there is only a weak mutual interference, and so the powder behaves as a single particle, but the effect on the cluster remains.
Conclusions: The particle volume fraction and kinetic energy of the cluster retain an inverse proportional relationship while the cluster state continuously shifts to a lean scatter state.

1. Introduction

In microelectromechanical systems (MEMS) technology, there is often a need to understand the basic mechanism of a particle volume fraction to stabilize a cluster and the void ratio that causes scattering. For example, a suspension of carbon particles in air must gradually form a homogeneous cluster during the formation of a carbon nanotube, and the suspension of cells in a liquid must be independent of the micromanipulation of the cells. Consequently, determining whether these particles behave as a cluster or a single particle has been a problem for MEMS engineers.

When a suspension of powder in a flow inhomogeneously disperses it should exhibit one of three behaviors: (i) agglomeration when particles come into contact with one another; (ii) lean scattering when a particle is not fluid-dynamically affected by other particles, and can therefore be considered as sedimentation of a single particle; (iii) and cluster when particles are fluid-dynamically affected by other particles and are between the agglomerate and lean scatter states.

A spherical cluster study by Slack [1,2] found that when a large number of particles fall, they form a bowl-shaped cluster, and that the downward velocity of these clusters is faster than that of a single particle. From the micro-hydrodynamics of a sedimenting particle in creeping flow, it is known that the sedimentation velocity of a spherical blob (cluster) of particles in a low Reynolds number flow can be given as:

$$U = \phi(R/a)^2 U_S \tag{1}$$

where U is the average velocity of the cluster, U_S is the terminal velocity of an isolated particle (i.e., the Stokes velocity), ϕ is the volume fraction of particles inside a cluster, R is the gyration radius of the cluster, and a is the radius of an isolated particle ($R \gg a$). This equation is obtained through a simple balance of viscous and buoyancy forces; but although theoretically correct, does not really apply in the real world. The reason for this is that U/U_S does not approach 1 when ϕ nears zero (i.e., a single particle state), which led to Batchelor [3] deriving a predictive equation

* Corresponding author.
E-mail addresses: nakash@me.tut.ac.jp, nakash@sasebo.ac.jp (K. Nakashima).

http://dx.doi.org/10.1016/j.powtec.2015.09.022
0032-5910/

for U (Eq. (2)) by considering some of the mutual interferences between particles in a dilute dispersion of spheres when $r/a \leqq 8$ (where r is the distance between particles)

$$U = (1-6.55\phi)U_S. \tag{2}$$

Garside and Al-Dibouni [4] also obtained an experimental approximation (Eq. (3)) by observing the fluidization and sedimentation of uniformly sized spheres in a solid–liquid system:

$$U = \varepsilon^{4.14}U_S = (1-\phi)^{4.14}U_S \tag{3}$$

where ε is the void ratio. Brady and Durlofsky [5] further identified the asymptotic distributions of dimensionless average sedimentation rates as a function of volume fraction by deriving a predictive equation for U (Eq. (4)) for disordered suspensions under conditions of $\phi < 0.5$

$$U = \left\{1 + \phi - \frac{1}{5}\phi^2 - \frac{6}{5}\phi\left(\frac{5-\phi+\phi^2/2}{1+2\phi}\right)\right\}U_S. \tag{4}$$

There have also been some experiments that have given some consideration to the shape of the particle cluster. Marzocchella et al. [6] observed the fall of a two-dimensional columnar cluster and developed a predictive equation for the cluster velocity based on its initial diameter and void ratio. Noh [7] and Bush et al. [8] also observed the influence of properties such as cluster buoyancy, cluster size, terminal velocity and fall position on the cluster velocity through experiments on a particle cloud. The void ratio and volume fraction were notably absent from these properties, however, as these proved difficult to measure. Nevertheless, the void ratio and volume fraction are believed to be an important influential factor on the downward velocity of a cluster. In a previous experimental study, the change in velocity of a gas flow around a Group A particle (based on Geldart's diagram) falling down a vertical pipe was studied using a video camera [9]. By considering the force of gravity, buoyancy and fluid drag at the point at which the cluster first began to slow, it was determined that the limiting void ratio of a cluster was $\varepsilon = 0.994$. Based on these previous studies, it is evident that when a spherical particle cluster falls it is eroded from its outer end, resulting in a gradual increase in the void ratio (i.e., the particle volume fraction decreases). This eventually causes the cluster state to suddenly disappear, at which point the downward velocity slows. These events are considered to occur as a result of a decrease in the mutual interference between particles when the void ratio increases.

When the terminal velocity of a particle U_S is much greater than the flow velocity (i.e., $St \gg 1$, where St represents the Stokes number of the suspension), as is the case with massive particles (i.e., a high particle inertia), the physics of a suspension is governed by particle contact. If, on the other hand, U_S is nearly equal to the flow velocity (i.e., St is nearly equal to 1), then the particles exhibit varied motions depending on the flow and often stagnate in the fluid either on their own or as part of a particle cloud. Finally, when U_S is much less than the flow velocity (i.e., $St \ll 1$), as is the case when small particles are immersed in a high viscosity fluid, the physics are governed by long-range slow decay hydrodynamic interactions. In the case of both $St \gg 1$ and $St \ll 1$, a steady flow can be assumed; but when $St \cong 1$, the particles exhibit an unsteady motion that is affected by flow and so it is thought that under these conditions the void ratio determines whether a cluster exists or not. However, it is known that these hydrodynamic interactions are related to $1/r$ [3], with r being the distance between two arbitrary particles. Given this, even if the void fraction of the suspension is increased the particles may still "feel" the presence of their neighbors. There is therefore a need to understand the critical characteristics that the void ratio imparts on the inertia of particles (or clusters), which requires looking at the motion of particle clusters that is caused only by low Reynolds number flow. This should make it possible to determine the characteristics defining whether particles exist as a cluster or not.

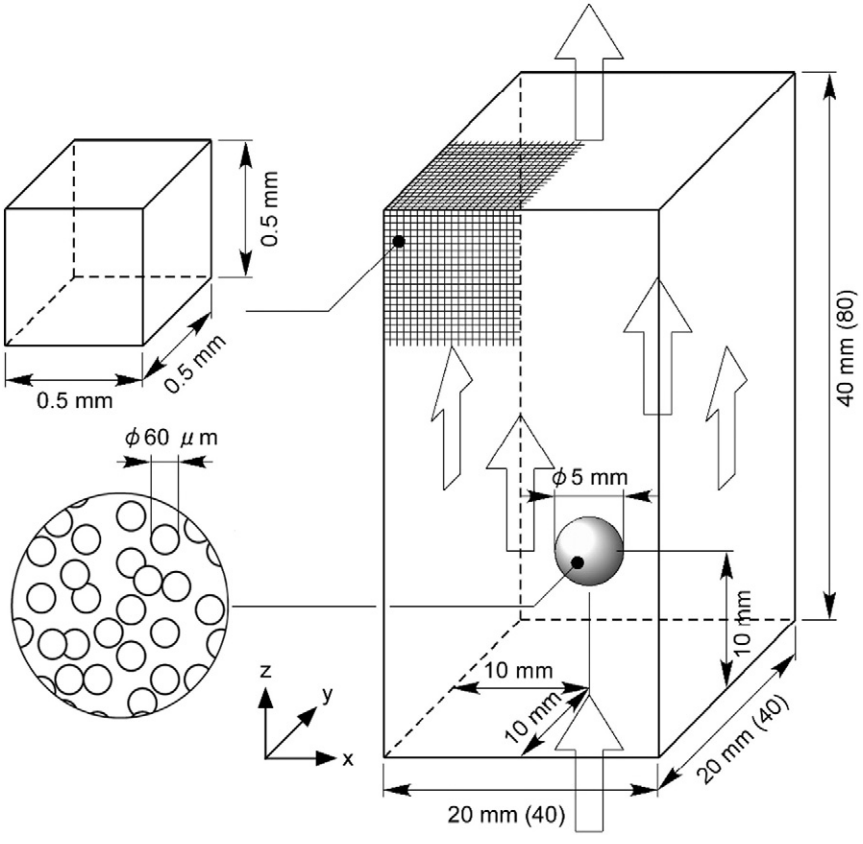

Fig. 1. Calculation domain.

There have been some past experiments that have focused on the void ratio of a spherical cluster in a fluidized bed, with Horio et al. measuring the meso-scale structure of fast fluidized suspensions using optical fiber techniques [10–13] and laser sheet methods [14–16]. In this manner, they were able to calculate the cluster diameter and void ratio by assuming a cluster-bubble model [17], observing a maximum void ratio of $\varepsilon = 0.92$ at cluster diameter of 4.3 mm. The calculated maximum void ratio based on the measurement results was $\varepsilon = 0.9986$, meaning that the maximum ε value needed to maintain a cluster was approximately 0.99. When the powder has a void ratio that is higher than this maximum, the particles should behave as single particles (dilute regime). Gudipaty et al. [18] also performed an experiment on the formation and growth of a cluster in a microchannel flow, from which they suggested that the flow rate and void ratio are the main factors controlling cluster formation. Conversely, no clear correlation was found between the void ratio and cluster size in the study of Horio and Ito [17]; however, dynamic relationships were expected to exist between the void ratio and velocity in the studies of both Horio and Ito [17] and Gudipaty [18].

Several visualization studies of particle clusters in a fluidized bed using high-speed cameras [19–22] or numerical simulation [23–27] have revealed that particle clusters typically take on an upward-paraboloid, downward-paraboloid or thin-film shape (the bowl-shaped cluster observed by Slack [2] corresponds to a downward-paraboloid). Abade and Cunha [26] performed computer simulations of particle aggregates during sedimentation that were similar to the particle cloud studied by Noh [7] and Bush et al. [8], but used a one-way method to develop a numerical scheme for a polydisperse blob suspended in a Newtonian fluid under gravity. Uchiyama [27] also simulated the fall of a spherical particle cluster using the vortex-in-a-cell method, and in doing so demonstrated the bowl-shaped cluster-generation process.

The formation of a cluster is believed to start with particles and fluid moving together to form something that behaves fluid-dynamically as a rigid sphere. Thus, in order to understand the conditions required to form or disperse a cluster during mechanical powder handling, the present study investigates the dynamic structure of particle clusters using numerical analysis. Focus is initially given to the void ratio needed to create a cluster and the transition process from a cluster state to a lean scatter state. Attention is then given to the fluid–dynamic energy budget, including that of the cluster, in order to better understand the mechanism by which fluid energy is converted to particle kinetic energy.

2. Calculation method and conditions

As this study examines the decrease in mutual interference between particles with increasing cluster void ratio, numerical simulations were conducted of a spherical particle cluster subjected to a uniform flow. In the initial state of the calculation the cluster stands still in air, but once the calculation starts, all velocity boundary conditions are imposed on the air-flow velocity until it asymptotically increases to terminal velocity. Gravity is not considered in the basic equations of the simulation for two reasons: to observe the cluster at a fixed point and to save calculation resources.

Table 1
Calculation conditions.

	Property	Value used
Particle	Diameter	60 μm
(glass bead)	Density	2.5×10^3 kg/m^3
	Terminal velocity	0.272 m/s
	Coefficient of restitution	0.9
	Coefficient of friction	0.3
Fluid	Density	1.20 kg/m^3
(air, 20 °C, 1 atm)	Viscosity	1.80×10^{-5} Pa·s
Calculation	Time step	2.5×10^{-6} s
	Cell size for fluid motion	$0.5 \times 0.5 \times 0.5$ mm

Table 2
Initial conditions of the cluster.

Void ratio ε	Number of particles	Cluster diameter
0.850	86,805	5.0 mm
0.920	46,296	
0.960	23,148	
0.980	11,574	
0.995	2,893	
0.998	1,157	

2.1. Calculation method for flow

The direct numerical simulation for a gas–solid flow of Tsuji et al. [23] was used in the flow calculation. The continuity equation and Navier–Stokes equation that considers the existence of particles were calculated using the marker-and-cell method. The basic equations of the calculation are as follows:

Non-dimensional continuity equation:

$$\frac{\partial \varepsilon}{\partial t} + \nabla \cdot \varepsilon \mathbf{u} = 0. \tag{5}$$

Non-dimensional Navier–Stokes equation:

$$\varepsilon \frac{\partial \mathbf{u}}{\partial t} + (\varepsilon \mathbf{u} \cdot \nabla)\mathbf{u} = -\nabla \varepsilon \; p - \frac{1}{Re} \nabla \cdot \varepsilon \boldsymbol{\tau} - \mathbf{S_p} \tag{6}$$

where t is the time, $\mathbf{u}$ is the air velocity vector, p is the static pressure, Re is the Reynolds number, $\boldsymbol{\tau}$ is the viscous stress tensor, and $\mathbf{S_p}$ is the drag force caused by particles. The term $\mathbf{S_p}$ in Eq. (6) is calculated using the Wen and Yu equation when there is a high void ratio, and the Ergun equation in the case of a low void ratio [28]. When the Reynolds number is low, the drag coefficient C_D in the Wen and Yu equation is calculated using the Schiller and Naumann equation [29]:

$$\mathbf{S_p} = \beta(\mathbf{u} - \bar{\mathbf{v}}_p) U_S / \rho. \tag{7}$$

This requires that

$$\beta = \begin{cases} \dfrac{\mu(1-\varepsilon)}{a^2 \varepsilon} \{150(1-\varepsilon) + 1.75 Re_p\} & (\varepsilon \le 0.8) \\ \dfrac{3}{4} C_D \dfrac{\mu(1-\varepsilon)}{a^2} \varepsilon^{-2.7} Re_p & (\varepsilon > 0.8) \end{cases} \tag{8}$$

$$C_D = \begin{cases} 24\left(1 + 0.15 Re_p^{0.687}\right)/Re_p & (Re_p \le 1000) \\ 0.43 & (Re_p > 1000) \end{cases} \tag{9}$$

$$Re_p = \varepsilon \frac{\rho a |\bar{\mathbf{v}}_p - \mathbf{u}| U_S}{\mu} \tag{10}$$

where $\bar{\mathbf{v}}_p$ is the mean velocity of the particles included in a calculation cell, ρ is the air density, and μ is the viscosity coefficient of the air.

Table 3
Details of the numerical platform.

	Details
Code (compiler)	Fortran (FUJITSU Software Fortran & C Package)
OS system	Linux 2.6
CPU	AMD Opteron 8220 (2 core, 2.8 GHz)
Memory	8 GB

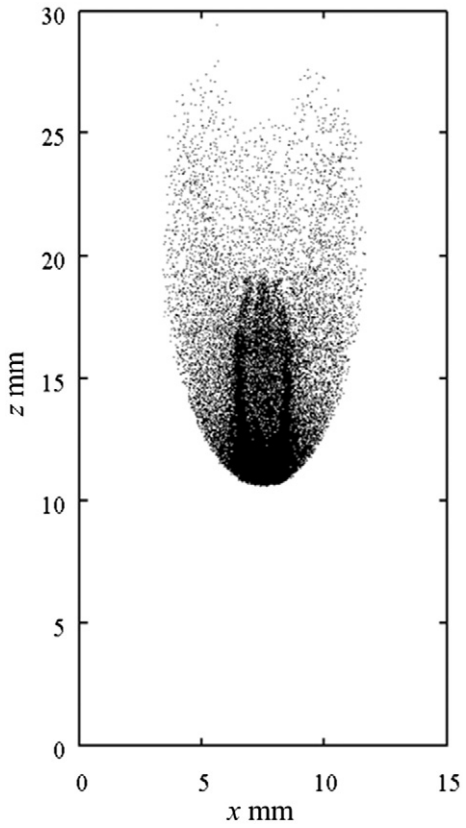

Fig. 2. Particle position map for $\varepsilon = 0.657$ after an elapsed time of 0.110 s. The vertical and horizontal axes are the real scale in mm. This result is similar to a photograph taken by Slack [2].

2.2. Calculation method for particle motion

The particle translation is calculated based on Newton's motion equation, which considers fluid drag force as

$$m_{pi}\frac{d\mathbf{v}_{pi}}{dt} = 3\pi\mu a(\mathbf{u}-\mathbf{v}_{pi})\left(1+0.15\mathrm{Re}_p^{0.687}\right) \tag{11}$$

where m_{pi} is the mass of one particle, $\mathbf{v}_{pi}$ is the particle velocity and the subscript i is the integer number that was assigned to each particle. The motion of the air and particle are linked through the interaction term $\mathbf{S_p}$ in Eq. (7) and right side term in Eq. (11). Particle trajectories were calculated with an equation for Lagrangian particle motion [30].

A hard-sphere model [31] is used for the collision among particles, i.e., the momentum of collisions between two neighboring particles was solved by Eq. (12). The validity of using this model is explained later in Section 2.5

$$m_{pi}\mathbf{v}_{pi}\big|_t + m_{pj}\mathbf{v}_{pj}\big|_t = m_{pi}\mathbf{v}_{pi}\big|_{t+\Delta t} + m_{pj}\mathbf{v}_{pj}\big|_{t+\Delta t}. \tag{12}$$

Here, Δt is the time step in the simulation. This program was coded in Fortran several years ago, and has been described in previously released results [32,33].

2.3. Calculation domain

Fig. 1 provides an outline of the calculation domain, in which the upper left figure shows the calculation grid of the air flow, and the length of all sides is 0.5 mm. The calculation domain on the right-hand side is a rectangular parallelepiped that lengthens in the direction of flow and has a size of 20 mm × 20 mm × 40 mm made up of 40 × 40 × 80 grids. The spherical cluster with a diameter of 5.0 mm is structured by 60-μm-diameter spherical particles and is located in the lower part of the calculation domain. In the initial state of the calculation, the center of the cluster was placed at the center of the x–y plane at a distance of one-quarter of the domain size from the bottom of the z-direction.

2.4. Boundary condition

The velocity of the 60-μm particle increased asymptotically and unsteadily from zero to the terminal velocity in all boundary conditions. The velocity used for the boundary condition was calculated using an explicit method based on a one-dimensional motion equation that considers gravity, buoyancy, and fluid drag [9]. In the calculation, the Morsi and Alexander equations [34] were used for the particle drag coefficient. The reasons for the provision of terminal velocity to a single-particle in the boundary condition were as follows: if a spherical cluster remains at the initial position, it shows which individual particles are affected from the other neighboring particles through the fluid–dynamic interference. This can therefore confirm whether the particles form a cluster. In contrast, if a particle cluster moves at the same velocity as the air flow, no mutual interference occurs and it can be confirmed that movement is as individual, single particles.

2.5. Calculation conditions

Table 1 lists the calculation conditions used. In the numerical calculation, the particles were assumed to be glass beads with a diameter of 60 μm, and the fluid to be air at 20 °C. If the time step size is too great then too many particles make contact during the calculation and the simulation loses reality. The calculation was therefore programmed to terminate when the number of particles in any one air-flow grid exceeded the maximum number that can geometrically exist in the grid. When test calculations were performed, the maximum time step size in which the calculation could be normally finished was generally found to be 5.0×10^{-6} s. The time step size of the main calculation used for this study was therefore set to 2.5×10^{-6} s to ensure the reliability of the calculation results.

Table 2 lists the initial conditions of the cluster. Six types of void ratios were selected from the range $0.657 < \varepsilon < 1$, and calculations were performed for each type. The positions of the particles in the cluster were randomly numerically determined. At around the calculation end time, each calculation was carried out until the velocity of the boundary condition reached approximately 99% of the terminal

Table 4
Experimental data and values calculated based on observation.

Experiment	Cluster void ratio ε	Cluster diameter	Equipment
Horio et al. (1988) [10]	0.86–0.92 obs.[a]	4.0–4.3 mm obs.	Fluidized bed
Horio et al. (1992) [13]	0.83–0.91 obs.[a]	4.4–14.3 mm obs.	Fluidized bed
Ito et al. (1995) [16]	0.9982–0.9986 cal.[b]	10–40 mm obs.	Fluidized bed
Nakashima et al. (2009) [9]	0.994 cal.[c]	18 mm obs.	Vertical pipe

[a] Observed using an optical fiber probe [10,13].
[b] Predicted based on force balance equations and geometrical considerations by assuming a cluster–bubble model [17].
[c] Predicted based on the force balance equation by assuming cluster cancelation (limit of void ratio) [9].

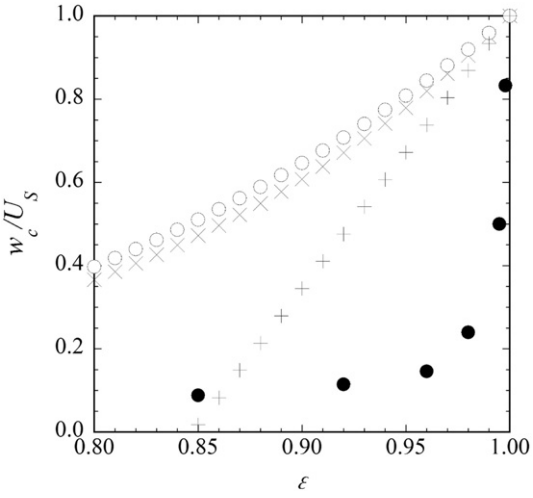

Fig. 3. Effect of initial void ratio on the instantaneous velocity ratio of a cluster vs. air flow. Points indicated by a ● correspond to calculations at an elapsed time of 0.08 s, a + corresponds to theoretical results (Eq. (2)) for sedimentation in a dilute dispersion of spheres (Batchelor [3]), a ○ corresponds to experimental results (Eq. (3)) for fluidization and sedimentation in a solid–liquid system (Garside and Al-Dibouni [4]), and a × corresponds to theoretical results (Eq. (4)) from a Rotne–Prager approximation of a Percus–Yevick hard-sphere distribution during the sedimentation of a disordered suspension (Brady and Durlofsky [5]).

velocity. Under these conditions, the range of the cluster Reynolds number is $Re \leq 89.3$, while the range of the particle Reynolds number is $Re_p \leq 1.08$ based on the maximum velocity of the boundary condition. This was verified by an additional calculation, which found that the percentage of particles in contact with each other is 0.827% when $\varepsilon = 0.85$, which was the highest volume fraction used. It was also found that if three particles are in contact at the same time, the percentage is 0.012% (the number of particles is 10). Given this low probability of three particles contacting, a hard-sphere model was used for the particle collision calculations. In other words, if more than three particles simultaneously make contact, only the collision of two particles with the largest contact amount is calculated. The average distance between particles was 6.67×10^{-5} m based on the assumption that 60 μm diameter particles form 5 mm diameter clusters with a 0.850 void ratio (86,805 particles).

Table 3 presents details on the numerical simulation, including the computational cost. The average time required for 0.08 s of simulation ($T = 0.08$ s) was less than 2 h, increasing to about 8 h before the cluster exceeded the calculation domain ($T = 0.19$ s and $\varepsilon = 0.657$). The map in Fig. 2 shows the position of all particles during the calculation conditions listed in the explanatory note of the figure. This demonstrates that the code used in this study is reliable as it does not fail even after a prolonged period of time, and produces results very similar to a photograph previously presented by Slack [2].

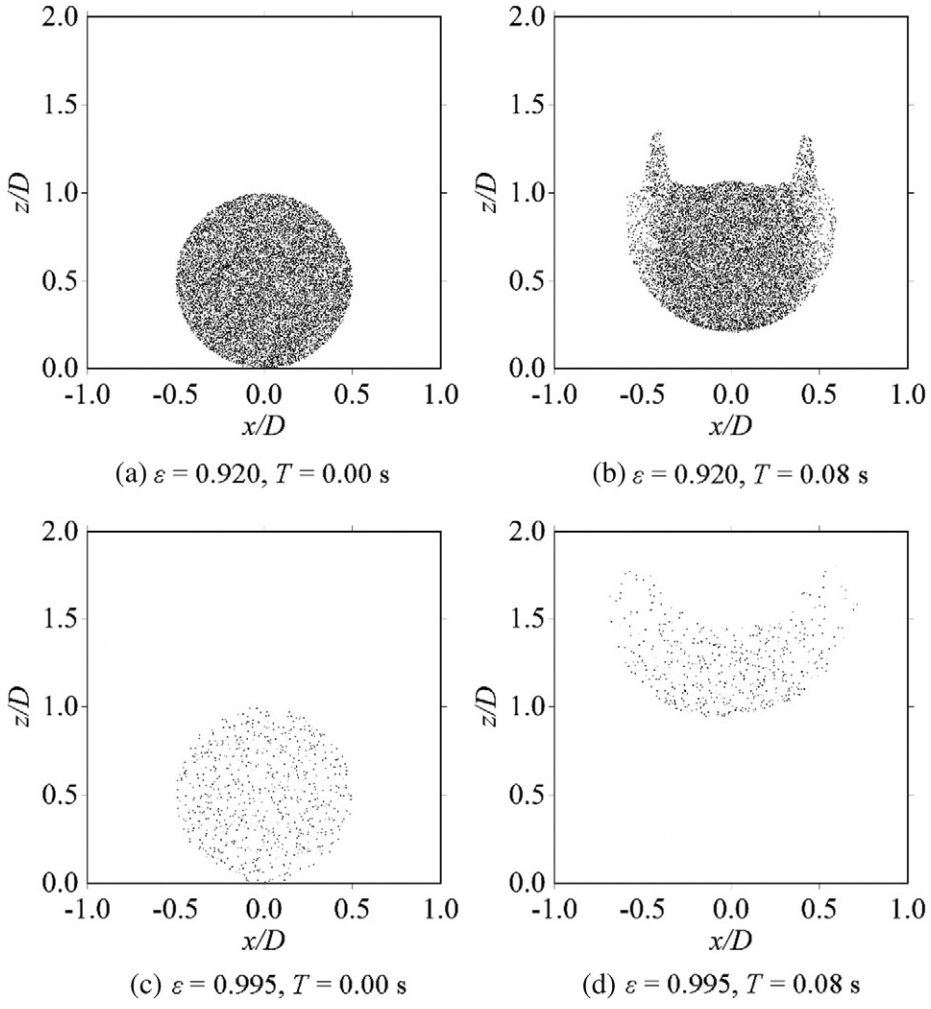

Fig. 4. Particle position maps of an x–z section at the center of the y-direction. (a) $\varepsilon = 0.920$, $T = 0.00$ s. (b) $\varepsilon = 0.920$, $T = 0.08$ s. (c) $\varepsilon = 0.995$, $T = 0.00$ s. (d) $\varepsilon = 0.995$, $T = 0.08$ s.

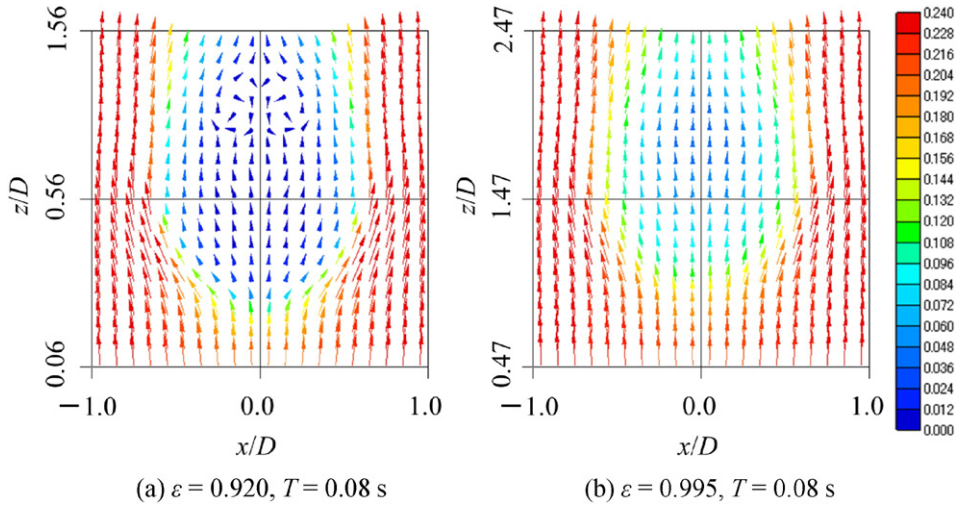

Fig. 5. Vector maps of air velocity at the central section (the number of vectors in both maps have been reduced to one-half the number of calculation cells). (a) $\varepsilon = 0.920$, $T = 0.08$ s. (b) $\varepsilon = 0.995$, $T = 0.08$ s.

3. Results and discussion

3.1. Void ratio and cluster velocity

In an experiment using a vertical pipe conducted by Nakashima et al. [9], the maximum void ratio of a cluster state was found to be maintained at $\varepsilon = 0.994$. This result suggests that there is a critical void ratio at which the flow influence suddenly becomes strong during the inhomogeneous dispersion of a powder suspension. Table 4 lists some of the measured and calculated values based on various past observations. In the measured values obtained by Horio et al. [10,13], $\varepsilon = 0.92$ is the maximum void ratio [10]. According to the predictive calculations based on a balance equation in which pressure gradient, buoyancy and gravity are considered, $\varepsilon = 0.9986$ is the maximum void ratio if a cluster–bubble model is assumed [17].

Fig. 3 shows the effect of the initial void ratio on the instantaneous velocity ratio of the cluster versus air flow based on the calculation results of the present study. Note that as the air-flow velocity is approximately equal to the terminal velocity, the cluster moves along the air-flow direction until it transformed from a sphere into a bowl shape. The instantaneous rising velocity of the cluster, w_c, is calculated by measuring its lowest position at each time interval. The vertical axis in Fig. 3 represents the instantaneous velocity ratio of the cluster versus air flow and demonstrates the effect of air flow on the cluster. The dimensionless parameter w_c/U_S represents the extent to which the cluster follows the air flow, and in this sense is similar to Stokes number. If the cluster is regarded as a whole structure, then w_c indicates by how much its velocity lags behind that of the flow. The difference between the terminal velocity lag velocity (i.e., $U_S - w_c$) represents the velocity at which the cluster can move by overcoming fluid drag. Because Stokes number can be considered a ratio between the terminal velocity of the particle and the characteristic velocity of the flow:

$$St \propto (U_S - w_c)/U_C \tag{13}$$

where U_C is the characteristic velocity of the flow. Moreover, as the focus here is on the micro critical unsteady characteristics of a cluster based on its void ratio, aspects of the flow velocity such as the superficial velocity of the fluidized bed can be ignored. For this reason, the dimensionless parameter w_c/U_S can be used as a substitute for Stokes number, thereby making it much easier to intuitively understand the simulation conditions. For example, a state of $w_c/U_S = 1$ means that the cluster moves with the air flow at the same velocity, and so is similar to a small particle immersed in a high viscosity fluid (i.e., $St \ll 1$).

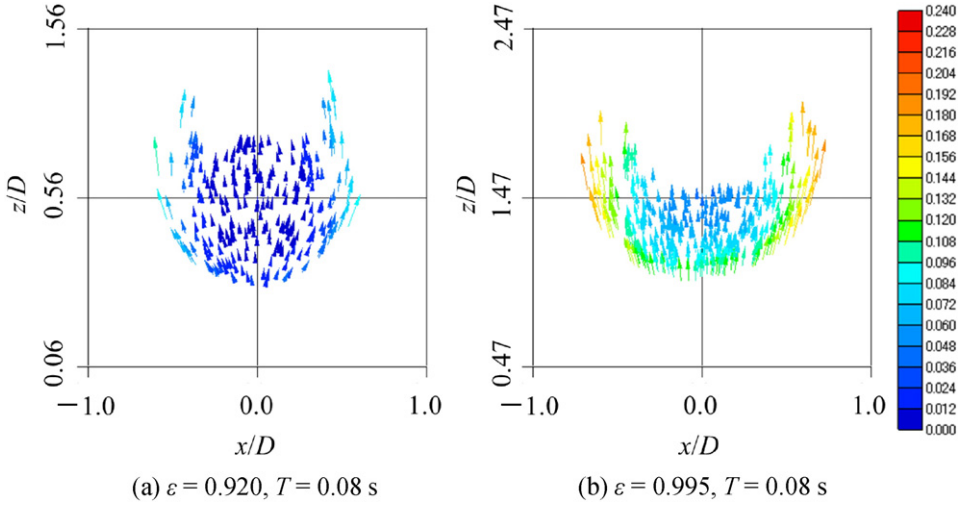

Fig. 6. Vector maps of particle velocity at the central section (the number of vectors in both maps have been reduced to (a) −1/40 and (b) one-half the number of particles in Fig. 4). (a) $\varepsilon = 0.920$, $T = 0.08$ s. (b) $\varepsilon = 0.995$, $T = 0.08$ s.

Conversely, a state of $w_c/U_S = 0$ means that the cluster completely stands still, and is therefore similar to a massive particle with high inertia in a low viscosity fluid (i.e., $St \gg 1$).

Simulation was carried out for each of the six different void ratios listed in Table 2; i.e., each plot point in Fig. 3 represents one simulation and all plot points represent the instantaneous velocity of a cluster at time $T = 0.08$ s (32,000 time steps). Literature data for dilute dispersions of spheres are also plotted in Fig. 3, which shows that the present calculations are similar to Batchelor's [3] theoretical result at around $\varepsilon = 0.85$. However, they are notably lower than the experimental results of Eq. (3) obtained by Garside and Al-Dibouni [4] and the theoretical values of Eq. (4) reported by Brady and Durlofsky [5]. Nevertheless, this shows the validity of a simulation code in which w_c/U_S doesn't exceed 1.0 at any point, and in which plot points asymptotically approach $\varepsilon = 1.00$.

Though Horio et al. [10,13] used the light reflected from an optical fiber probe to determine the void ratio of clusters in a fluidized bed, the difficult in obtaining accurate measurements means that these are at best a rough estimate [12]. Nevertheless, they found that a cluster void ratio of $0.83 < \varepsilon < 0.92$ [10,13] produces a stable cluster due to a minimal increase in w_c/U_S. This low value of w_c/U_S means that there is a high extent of mutual interference between particles, resulting in large clusters. Horio et al. [17] have also suggested a cluster bubble model and predicted cluster void ratios based on the experimental results of Ito et al. [16], which gave a cluster void ratio range of $0.9982 < \varepsilon < 0.9986$ [17]. Similarly, the void ratio at which clusters are canceled in a vertical pipe has been predicted to be 0.994 [9], suggesting that the upper limit of the void ratio is about 0.99. This compares well with the void ratio predicted from the simulation results in Fig. 3 of about 0.99 based on the fact that w_c/U_S suddenly increases when the void ratio becomes larger than $\varepsilon = 0.960$ to 0.980, which is believed to represent a change from a stable to unstable cluster. Unfortunately it would be very difficult to reproduce the calculation conditions experimentally, thus making it impossible to plot a distribution of experimental values similar to that shown in Fig. 3.

If we consider the simulation as a real free fall (for example, that in Slack [1,2] and Marzocchella et al. [6]) in the range $\varepsilon < 0.960$, then the particles should behave as a cluster with an inertia sufficient to overcome the air resistance; i.e., a cluster that can move in a fluid. On the other hand, a value of $\varepsilon > 0.980$ represents a state in which the distance between particles is large, meaning that individual particles encounter flow resistance and move with the air flow, eventually being blown off and scattered in a manner similar to that observed in an experiment by Nakashima et al. [9].

3.2. Visualization of flow structure

Two representative cases are examined from the visualized maps: the state where the particles behave as a cluster, and where they lose mutual interference. Fig. 4(a)–(d) contains the particle position maps obtained from a x–z section at the center of the y-direction. Fig. 4(a) shows the initial state of the calculation at $\varepsilon = 0.920$, with only those particles that exist in the two calculation grids and make contact in the x–z central section (depth is 1 mm and range is $-0.1 < y/D < 0.1$) being shown, and D indicating the cluster diameter. Fig. 4(b) shows the calculation result at $T = 0.08$ s (32000 time steps) using the same plot conditions as in Fig. 4(a). For the number of particles shown in both Fig. 4(a) and (b), the number of plot points is 12,493. Thus, when Fig. 4(b) is compared with Fig. 4(a), we find that the bottom end of the cluster moves up to 0.92 mm ($z/D = 0.184$; this value was measured using an enlarged picture). In addition, we find that the cluster is transformed from its initial state, eroding near $x/D = \pm 0.5$ and being scattered upward. Fig. 4(c) demonstrates the initial state of the calculation at $\varepsilon = 0.920$ and again uses the same plot conditions as Fig. 4(a) and (b), albeit with only 626 particles displayed in the map. Nevertheless, the position of the whole cluster at the initial state is clearly the same as that shown in Fig. 4(a). Fig. 4(d) shows the calculation result at $T = 0.08$ s (32,000 time steps), and when compared with Fig. 4(c), we find that the bottom end of the cluster moves upward to 4.46 mm [$z/D = 0.892$, measured similar to Fig. 4(b) using an enlarged picture]. The amount of cluster movement is far more pronounced in Fig. 4(d) than (b), which suggests that the state depicted in Fig. 4(d) has lost most of the mutual influence among particles, and so the effect this has on clusters has disappeared. Moreover, Fig. 4(d) is similar to the gentle paraboloid shape in the particle cloud photographs taken by Noh [7] and Bush et al. [8], and which has also been observed in the numerical simulation results of Uchiyama [27] at a 0.025 volume fraction condition.

Fig. 5 presents an air-flow vector map of the central cross section, with Fig. 5(a) showing the calculation result at $T = 0.08$ s when $\varepsilon = 0.920$. The velocity at the boundary condition at this time is 0.270 m/s, and

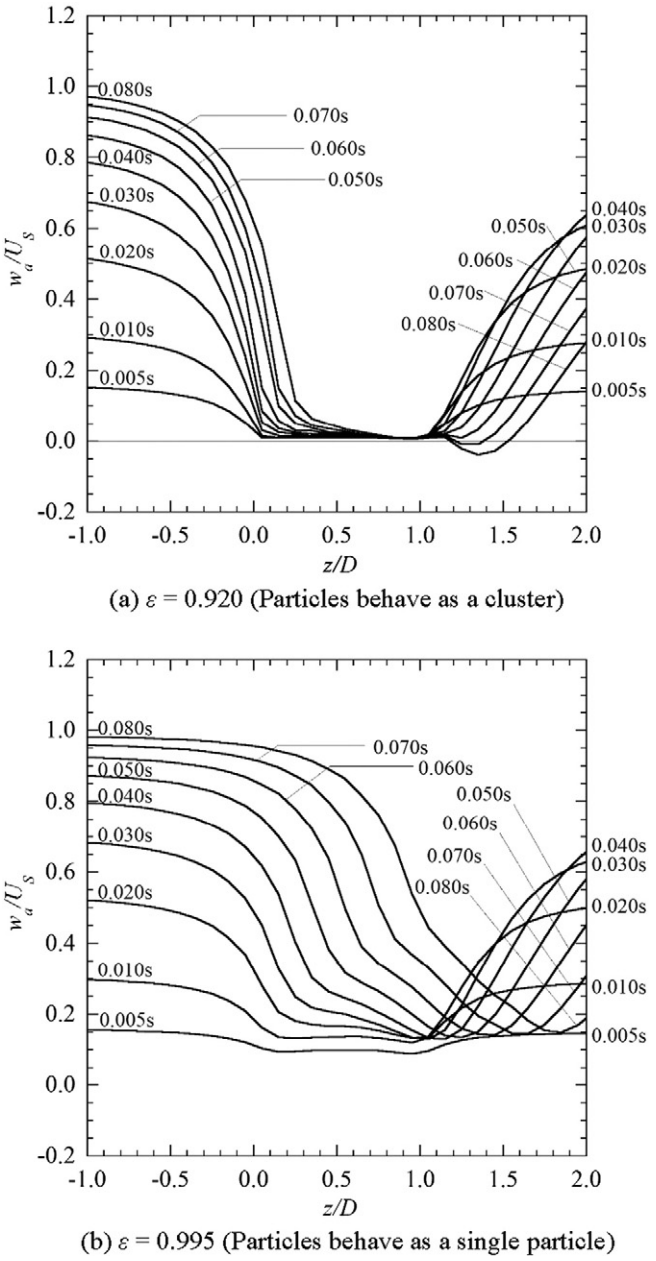

Fig. 7. Instantaneous air velocity distributions on the central axis in the flow direction. Velocity distributions for each time interval are progressively plotted in the range of $0.005\text{ s} < T < 0.080\text{ s}$. (a) $\varepsilon = 0.920$ (particles behave as a cluster). (b) $\varepsilon = 0.995$ (particles behave as a single particle).

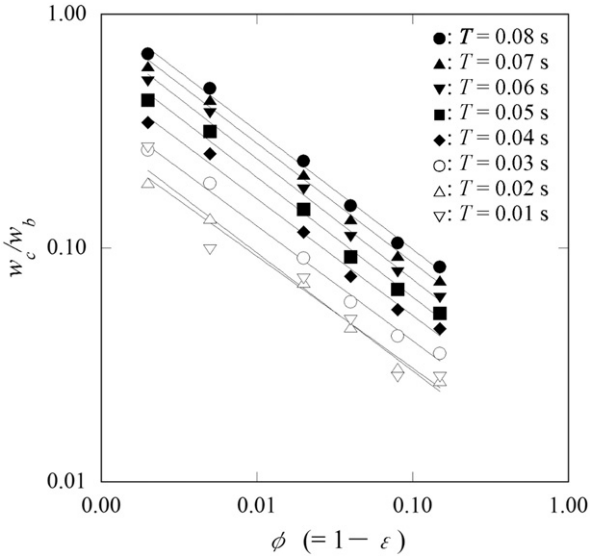

Fig. 8. Relationship between the initial particle volume fraction ϕ and the degree of influence w_c/w_b that the air velocity has on the cluster velocity.

$Re = 89.3$ based on the cluster diameter and boundary condition velocity. The flow shown in Fig. 5(a) thus very much resembles the flow around a rigid ball set in a uniform flow. Because the distances between particles are small and air cannot pass through the particles, the cluster fluid-dynamically behaves like a rigid sphere. Involute vortexes are found near $z/D = 1.2$ at the center in the x-direction. Fig. 5(b) shows the calculation result at $T = 0.08$ s when $\varepsilon = 0.995$, conditions under which we believe that the cluster moves with the air flow; however, an air-flow movement that avoids the cluster is simultaneously observed near $-0.7 < x/D < 0.7$ and $0.9 < z/D < 1.3$. Based on these results, it would seem that although the particles lose the effect of staying as a cluster, some of these effects are retained.

Fig. 6 contains a particle vector map of the central cross section, with Fig. 6(a) showing the calculation results at $T = 0.08$ s when $\varepsilon = 0.920$. Note that the number of particles is randomly reduced from 12,493 to 312, which is due to the cluster being eroded by the air flow near $x/D = \pm 0.5$ and $z/D = 0.75$ and particles being scattered upward. In the air flow that avoids the sphere, the velocity becomes a maximum at the sides of the sphere. As Bernoulli's theorem dictates that an increase in velocity is accompanied by a pressure decrease, this allows particles to more easily leave the cluster. Fig. 6(b) shows the calculation results at $T = 0.08$ s when $\varepsilon = 0.995$, in which the number of particles is randomly reduced from 626 to 312 and almost all particles move upward. Interestingly, particles under the surface and at the side of the cluster have a high velocity, suggesting that a steadily increasing flow causes a rapid increase in the viscous drag force. This in turn accelerates the rate of powder scattering with very little interference among particles, meaning that each particle most likely moves independently in the fluid. Sobral et al. [35] have previously discussed similar unsteady characteristics during the motion of a falling particle by considering some of the forces acting on it, namely the viscous drag force, Basset force, virtual mass drag force and Oseen approximation term. This found that in the case of gas–solid flow the viscous drag force and Basset force are dominant factors in the initial motion of a particle. That is, when the flow velocity is low, the Basset force acts to disturb the particle's acceleration motion through the drag induced by the trailing vortex. However, when the flow velocity increases to a sufficient level, particles leave the trailing vortex. This results in a gradual decrease in the influence of the Basset force and a rapid increase in the influence of viscous drag. It should be noted here that although the trailing vortex is opposite to the direction of a moving particle in the case of sedimentation, it is in the same direction in the simulation used in this study. Consequently, the distribution of results in Fig. 3 may be different from other theoretical and experimental results, as the present results only show the critical characteristics caused by fluid viscous drag.

The bowl-shaped cluster at $\varepsilon = 0.920$ is caused by airflow erosion at the outer end of the cluster; i.e., as the cluster behaves as a rigid sphere, any eroded particles are carried with the airflow around the sphere. The gentle paraboloid shape at $\varepsilon = 0.995$, on the other hand, is the result of independent particle motion within the cluster. In other words, each particle moves under the influence of air flow z-direction because they have lost any significant mutual interference. As there is a slight leftward bias created by the outward airflow, a gentle paraboloid shape is produced. The results in this section can therefore be summarized as follows: when particles attain a cluster state, a flow structure around a rigid sphere is formed around the whole spherical cluster. The subsequent increase in flow-velocity and decrease in pressure causes particle scattering and erosion on the cluster sides.

3.3. Air permeability of the cluster

Fig. 7(a) and (b) shows the distribution of dimensionless air-flow velocity on the central axis, with this being calculated by dividing the instantaneous air-flow velocity by the terminal velocity. The value w_a is the instantaneous air velocity. These figures reveal that when $\varepsilon = 0.920$ there is a notable interference among particles and the air flow does not pass through the cluster in the central axis because w_a/U_S near $z/D = 1.0$ is approximately zero at all times. In addition, w_a/U_S becomes negative at $T = 0.080$ s near $z/D = 1.35$. This indicates that an involute vortex is generated at the rear of the cluster because a flow around the sphere is formed. In Fig. 7(b), it is evident that there is very little interference among the particles when $\varepsilon = 0.995$ because the air

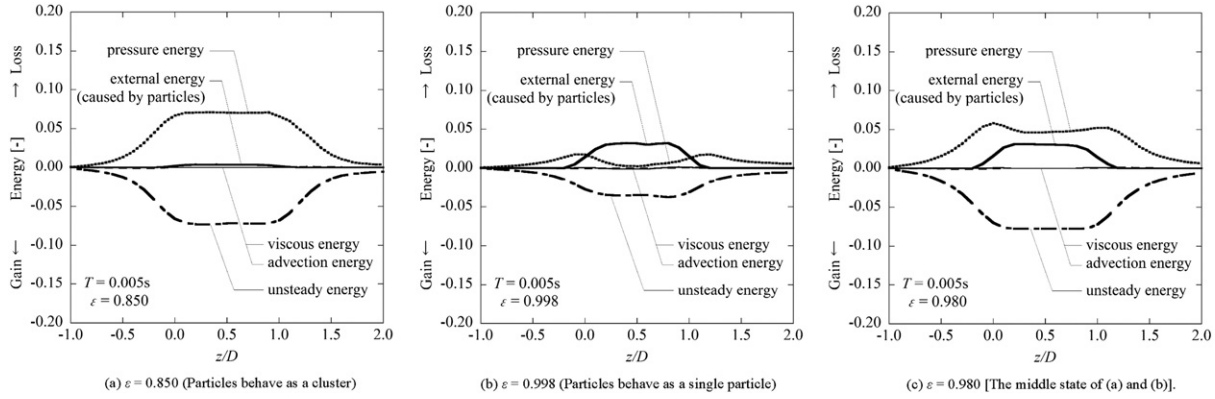

(a) $\varepsilon = 0.850$ (Particles behave as a cluster) (b) $\varepsilon = 0.998$ (Particles behave as a single particle) (c) $\varepsilon = 0.980$ [The middle state of (a) and (b)].

Fig. 9. Instantaneous flow energy budget on the central axis. Plotted points represent results obtained immediately after the start of calculation at $T = 0.005$ s. (a) $\varepsilon = 0.850$ (Particles behave as a cluster). (b) $\varepsilon = 0.998$ (particles behave as a single particle). (c) $\varepsilon = 0.980$ [the middle state of (a) and (b)].

flow acquires velocity just after the very start of the calculation ($T = 0.005$ s). However, a slowdown in the air-flow velocity is observed at all time intervals due to the existence of a cluster in $z/D > 0.0$. Thus, although the fluid–dynamic interference among particles is very small, its effect on clusters remains.

3.4. Degree of air flow influence on clusters based on velocity

Fig. 8 shows the relationship between the initial particle volume fraction ϕ and the degree of influence w_c/w_b that the air velocity has on the cluster velocity. The vertical axis is a dimensionless quantity that divides the instantaneous cluster velocity w_c by the instantaneous air velocity at the boundary condition w_b. Each instantaneous cluster velocity plotted was obtained from the visualization results using the same method shown in Fig. 3. With regard to the distribution at $T = 0.080$ s (marked as ● in Fig. 8), if we extend the straight line to the $\phi = 0$ side then we find that the intersection point with the vertical axis is $w_c/w_b = 1.00$ ($w_c = w_b$). The state in which the air-flow and cluster velocities are equal in this simulation represents conditions where the fluid drag and other external forces are balanced under the theorem of single-particle sedimentation. Thus, the results in which the cluster and air-flow velocities are equal are dynamically correct when the particle volume fraction approaches zero. Even if particles did collide, the particle velocity cannot be higher than the air flow velocity, thereby verifying the reliability of the calculation code. It can also be seen that the velocity ratio w_c/w_b and particle volume fraction ϕ are linearly correlated at all times, and that the slopes of these straight lines are approximately 0.5. In other words, the particle volume fraction has an inverse proportional relationship with the kinetic energy of the cluster, as expressed by Eq. (14)

$$\phi \cdot \left(\frac{w_c}{w_a}\right)^2 = const. \tag{14}$$

3.5. Fluid–dynamic energy balance of the cluster

This section presents an examination of the energy balance between the air flow and particles. The energy budget equation is related to the derivation of Hinze [36], and can be expressed as Eq. (15) by multiplying both sides of the Navier–Stokes by an air-flow vector:

$$\varepsilon \frac{\partial}{\partial t}\left(\frac{1}{2}\mathbf{u}\cdot\mathbf{u}\right) + \varepsilon\mathbf{u}\cdot\nabla\left(\frac{1}{2}\mathbf{u}\cdot\mathbf{u}\right) = -\mathbf{u}\cdot\nabla\varepsilon p + \frac{1}{Re}\mathbf{u}\cdot(\nabla\cdot\varepsilon\boldsymbol{\tau}) - \mathbf{u}\cdot\mathbf{S_p}. \tag{15}$$

Fig. 9(a)–(c) shows the distribution of each term in Eq. (15) on the central axis, with these representing the unsteady, advection, pressure, viscous and external energies (caused by particles). It is apparent from this that a cluster exists in the range $0.0 < z/D < 1.0$, and that the unsteady and pressure energies offset each other; thus, all energies are zero at $z/D = -1.0$. The simulation results can therefore be considered equivalent to the free fall of a cluster. Fig. 9(a) shows the case when $\varepsilon = 0.850$ (i.e., the cluster void ratio is low), and so if we imagine a free falling rigid sphere understanding these results becomes easy. That is, the pressure energy increases toward position $z/D = 0.0$, which represents a stagnation point created by the fact that the air flow cannot pass through the cluster. The unsteady energy, which is a time derivative of the kinetic energy, also clearly decreases as the pressure energy increases. This means that that although the external energy due to the particles is very small, it is still larger than the viscous and advection energies. Fig. 9(b) presents the case when $\varepsilon = 0.998$ (i.e., the cluster void ratio is high), in which we see that each particle does not encounter fluid–dynamic interference from other particles and instead behaves almost independently. The pressure and particle energies therefore cross the stagnation point $z/D = 0.0$, and the particles are only affected by the air flow with an increase in the void ratio and subsequent push by the increased pressure. This means that of the fluid–dynamic energies only the pressure energy provides energy to the particles. Collectively, because the air flow approaches the stagnation point of the cluster, the kinetic energy decreases and the pressure energy simultaneously increases. Furthermore, when the air flow passes through a cluster, most of the increased pressure energy is used as kinetic energy by the particles. Fig. 9(c) shows the case when $\varepsilon = 0.980$, which represents a middle state between (a) and (b), and here we find that part of the pressure energy is used as kinetic energy by the particles. From this, it can be concluded that the process that leads to a single-particle state from a cluster does not suddenly happen, but that the distribution ratio of each energy is a process of continuous change.

4. Concluding remarks

The void ratio at which particles can form a cluster has been investigated through direct numerical simulation of a spherical cluster subjected to a uniform flow. The relationship between the void ratio (or particle volume fraction) and the movement velocity of the cluster was primarily investigated.

According to the numerical simulation, we determined that the cluster suddenly disappeared when $\varepsilon = 0.960$ to 0.980. These simulations appeared realistic because this void ratio is approximately equal to the observed maximum in the literature (Horio et al. [10,13], Ito et al. [16], and Nakashima et al. [9]). Through our analysis of the simulation results, the following conclusions were drawn:

(i) The transition from a cluster to a single-particle state suddenly develops at ε of approximately from 0.960 to 0.980. However, the cluster continually changes to a state in which the particles behave independently similar to that of single-particle sedimentation.
(ii) The particle volume fraction is inversely proportional to the kinetic energy of the cluster during the powder-scattering process.

The mechanism of the critical phenomenon, i.e., the manner in which mutual interference among particles decreases with increasing cluster void ratio, was clarified. This is knowledge that is of great value to the latest in industrial powder handling applications, such as MEMS technology.

Acknowledgments

This work was financially supported by Sanko Machinery Co. and by Dr. M. Nakao (KAKEN, Research Project Number: 20224001), President of the National Institute of Technology, Sasebo College, Japan. The authors would like to express their heartfelt gratitude to Mr. T. Yamauchi, Mr. S. Kanazawa, and Mr. Y. Mizumoto for their cooperation in conducting the computer calculation and data reduction. They would also like to thank Editage (www.editage.jp) for providing English language editing.

References

[1] G.W. Slack, Sedimentation of compact clusters of uniform spheres, Nature 200 (1963) 466–467.
[2] G.W. Slack, Sedimentation of a large number of particles as a cluster in air, Nature 200 (1963) 1306.
[3] G.K. Batchelor, Sedimentation in a dilute dispersion of spheres, J. Fluid Mech. 52 (1972) 245–268.
[4] J. Garside, M.R. Al-Dibouni, Velocity–voidage relationships for fluidization and sedimentation in solid–liquid system, Ind. Eng. Chem. Process. Des. Dev. 16-2 (1977) 206–214.
[5] J.F. Brady, L.J. Durlofsky, The sedimentation rate of disordered suspensions, Phys. Fluids 31–4 (1988) 717–727.
[6] A. Marzocchella, U. Arena, A. Cammarota, Break-up of cylindrical clusters of solid particles under gravity flow in a two-dimensional column, Powder Technol. 65 (1991) 453–460.
[7] Y. Noh, Sedimentation of a particle cloud across a density interface, Fluid Dyn. Res. 27 (2000) 129–142.

[8] J.W.M. Bush, B.A. Thurber, F. Blanchette, Particle clouds in homogeneous and stratified environments, J. Fluid Mech. 489 (2003) 29–54.
[9] K. Nakashima, Y. Johno, T. Shigematsu, Free-fall characteristics of particle clusters in a vertical pipe, J. Phys. Conf. Ser. 147 (2009), 012070.
[10] M. Horio, K. Morishita, O. Tachibana, N. Murata, Solid distribution and movement in circulating fluidized beds, in: P. Basu, J.F. Large (Eds.), Circulating Fluidized Bed Technology II, Pergamon Press, Oxford, UK 1988, pp. 147–154.
[11] H. Ishii, T. Nakajima, M. Horio, The clustering annular flow model of circulating fluidized bed, J. Chem. Eng. Jpn. 22 (1989) 484–490.
[12] M. Horio, H. Ishii, M. Nishimuro, On the nature of turbulent and fast fluidized beds, Powder Technol. 70–3 (1992) 229–236.
[13] M. Horio, K. Mori, Y. Takei, H. Ishii, Simultaneous gas and solid velocity measurements in turbulent and fast fluidized beds, in: O.E. Potter, D.J. Nicklin (Eds.), Fluidization VII, Engineering Foundation, New York 1992, pp. 757–762.
[14] M. Horio, H. Kuroki, Three-dimensional flow visualization of dilutely dispersed solid in bubbling and circulating fluidized beds, Chem. Eng. Sci. 49 (1994) 2413–2421.
[15] H. Kuroki, M. Horio, The flow structure of a three-dimensional circulating fluidized bed observed by the laser sheet technique, in: Amos A. Avidan (Ed.), Circulating Fluidized Bed Technology IV, Proc. 4th Int. Conf. Circulating Fluidized Beds, Somerset, Pennsylvania, USA 1993, pp. 77–84.
[16] M. Ito, M. Tsukada, H. Kamiya, M. Horio, Three-dimensional meso-scale structure of gas solid suspensions in a circulating fluidized bed based on scanning laser sheet image analysis, Proc. 1st SCEJ Symposium on Fluidization, Tokyo, Japan 1995, pp. 177–184.
[17] M. Horio, M. Ito, Prediction of cluster size in circulating fluidized beds, J. Chem. Eng. Jpn. 30–4 (1997) 691–697.
[18] T. Gudipaty, M.T. Stamm, L.S.L. Cheung, L. Jiang, Y. Zohar, Cluster formation and growth in microchannel flow of dilute particle suspensions, Microfluid. Nanofluid. 10–3 (2011) 661–669.
[19] M. Rhodes, H. Mineo, T. Hirama, Particle motion at the wall of a circulating fluidized bed, Powder Technol. 70 (1992) 207–214.
[20] H. Hatano, N. Kido, Microscope visualization of solid particles in circulating fluidized beds, Powder Technol. 78 (1994) 115–119.
[21] M. Tsukada, M. Ito, H. Kamiya, M. Horio, Three-dimension imaging of particle clusters in dilute gas–solid suspension flow, Can. J. Chem. Eng. 75 (1997) 466–470.
[22] U. Lackermeier, C. Rudnick, J. Werther, A. Bredebusch, H. Burkhardt, Visualization of flow structures inside a circulating fluidized bed by means of laser sheet and image processing, Powder Technol. 114 (2001) 71–83.
[23] Y. Tsuji, T. Tanaka, S. Yonemura, Cluster patterns in circulating fluidized beds predicted by numerical simulation (discrete particle model versus two-fluid model), Powder Technol. 95–3 (1998) 254–264.
[24] T. Tsuji, A. Ito, T. Tanaka, Multi-scale structure of clustering particles, Powder Technol. 179 (2008) 115–125.
[25] M.H. Zhang, K.W. Chu, F. Wei, A.B. Yu, A CFD–DEM study of the cluster behavior in riser and downer reactors, Powder Technol. 184 (2008) 151–165.
[26] G.C. Abade, F.R. Cunha, Computer simulation of particle aggregates during sedimentation, Comput. Methods Appl. Mech. Eng. 196 (2007) 4597–4612.
[27] T. Uchiyama, Numerical simulation of particle-laden gas flow by vortex in cell method, Powder Technol. 235 (2013) 376–385.
[28] D. Gidaspow, Multiphase Flow and Fluidization-continuum and Kinetic Theory Descriptions, Academic Press, San Diego, 1994.
[29] V.L. Schiller, A. Naumann, ber die Grundlegen Berechnungen bei der Schwerkraftaufbereitung, Z. Ver. Dtsch. Ing. 77 (1933) 318–321.
[30] S. Yuu, K. Ikeda, T. Umekage, K. Nohara, Numerical simulation of three dimensional fluidized bed using nozzles at bottom and experimental verification, KONA 15 (1997) 190–201.
[31] J. Yan, K. Luo, J. Fan, Y. Tsuji, K. Cen, Direct numerical simulation of particle dispersion in a turbulent jet considering inter-particle collisions, Int. J. Multiphase Flow 34–8 (2008) 723–733.
[32] K. Nakashima, Y. Johno, F. Matsuyama, T. Shigematsu, Decrement characteristics of the mutual interference between the particles with the increase of the void ratio, 8th International Conference on Multiphase Flow ICMF 2013, Jeju, Korea, May 26–31, 2013 (ICMF2013-351).
[33] K. Nakashima, Y. Johno, T. Yamauchi, S. Kanazawa, Investigation of the flow characteristic of a spherical particle cluster in a uniform flow by numerical simulation, 29th Multiphase Flow Symposium, The Japanese Society for Multiphase Flow (JSMF) Annual Meeting 2010, Hamamatsu 2010, pp. 388–389 (in Japanese).
[34] S.A. Morsi, A.J. Alexander, An investigation of particle trajectories in two-phase flow systems, J. Fluid Mech. 55–2 (1972) 193–208.
[35] Y.D. Sobral, T.F. Oliveira, F.R. Cunha, On the unsteady forces during the motion of a sedimenting particle, J. Powder Technol. 178 (2007) 129–141.
[36] J.O. Hinze, Turbulence, 2nd edition McGraw-Hill Inc., USA, 1975.